Supporting Information

Construction of hydrophilic triazine-based covalent organic framework aerogels for enhanced adsorption and photocatalytic degradation of Congo Red

Haiping Liu, Yanyan Ren, Fang Duan, * Zhijian Pan, Qingqiu Huang, Shuanglong Lu and Mingliang Du

Key Laboratory of Synthetic and Biological Colloids, Ministry of Education, School of Chemical and Material Engineering, Jiangnan University, Wuxi 214122, P. R. China

Corresponding Authors. E-mail Addresses: duanfang@jiangnan.edu.cn (F. Duan) *

1. Materials

4,4',4''-(1,3,5-Triazine-2,4,6-triyl)trianiline (TZ), trialdehyde phloroglucinol (TP), and 1,3,5-triformylbenzene (BTCA) were purchased from Jilin Chinese Academy of Sciences–Yanshen Technology Co., Ltd. $Sc(OTf)_3$, Congo red (CR), p-benzoquinone (p-BQ), tert-Butanol (TBA), and disodium ethylenediaminetetraacetate (EDTA-2Na) were obtained from Shanghai Macklin Biochemical Technology Co., Ltd. Acetonitrile, tetrahydrofuran (THF), ethanol, hydrochloric acid (HCl), and sodium hydroxide (NaOH) were purchased from Sinopharm Chemical Reagent Co., Ltd. All commercially available solvents and reagents were of analytical grade and used without further purification.

2. Synthesis of COFs.

2.1 Synthesis of TTP-A

TZ (35.4 mg, 0.1 mmol) and TP (21.0 mg, 0.1 mmol) were dissolved in 1 mL of acetonitrile, respectively and ultrasonically dispersed, followed by mixing of the two solutions. Subsequently, 5 mg of $Sc(OTf)_3$ was added into the above mixed solution. The mixture rapidly turned turbid and gelled within a short time. The resulting system was sealed in a closed container and heated at 120 °C for 24 h. After the reaction, the products were immersed three times in excess tetrahydrofuran (THF), ethanol, and deionized water to remove unreacted species and impurities, respectively. After solvent exchange, the samples were freeze-dried overnight to obtain the corresponding yellow aerogel, denoted as TTP-A (49 mg, 94 % yield).

2.2 Synthesis of TTP-P

TZ (35.4 mg, 0.1 mmol) and TP (21.0 mg, 0.1 mmol) were dissolved in 1 mL of acetonitrile, respectively and ultrasonically dispersed, followed by mixing of the two solutions. Subsequently, 0.2 mL of 12 M acetic acid was added as a catalyst. The resulting mixture was sealed in a container and kept at room temperature for 3 days. After the reaction, the precipitate was collected by centrifugation and sequentially washed with tetrahydrofuran (THF), ethanol, and deionized water to remove the unreacted monomers and impurities, respectively. Finally, the sample was freeze-dried overnight to obtain the corresponding yellow powder, denoted as TTP-P (46 mg, 88% yield).

2.3 Synthesis of TCA-A

TZ (35.4 mg, 0.1 mmol) and BTCA (16.2 mg, 0.1 mmol) were dissolved in 1 mL of acetonitrile, respectively and ultrasonically dispersed, followed by mixing of the two solutions. Subsequently, 5 mg of $Sc(OTf)_3$ was added. The mixture quickly turned turbid and gelled within a short time. The resulting system was sealed in a closed container and kept at room temperature for 24 h. After the reaction, the products were immersed three times in excess tetrahydrofuran (THF), ethanol, and deionized water to remove unreacted species and impurities, respectively. After solvent exchange, the samples were freeze-dried overnight to obtain the corresponding light-yellow aerogel, denoted as TCA-A (43 mg, 90% yield).

3. Characterization

Scanning electron microscopy (SEM) images were obtained using a Hitachi S-4800 microscope. The compression test was measured by an electronic universal testing machine controlled by a microcomputer (MTS E44.304). Fourier transform infrared (FT-IR) spectra were recorded in the range of 4000–500 cm^{-1} using a Thermo Fisher spectrometer. Powder X-ray diffraction (PXRD) patterns were collected over a 2θ range of 2°–30° on a Bruker D8 Advance diffractometer. N_2 adsorption–desorption isotherms were measured at 77 K using a Micromeritics ASAP 2460 instrument. X-ray photoelectron spectroscopy (XPS) measurements were performed on a Thermo Scientific spectrometer with a monochromatic Al Kα X-ray source (hν = 1486.6 eV, 300 W), and the binding energies were calibrated with the C 1s peak at 284.8 eV. Solid-state ^{13}C NMR spectra were obtained on a Bruker 400 MHz spectrometer. Static

water contact angles were measured using a Theta Flow optical contact angle goniometer. Thermogravimetric analysis (TGA) was conducted on a METTLER TGA 2 analyzer under a nitrogen atmosphere from 50 to 800 °C at a heating rate of 10 °C min^{-1}. The concentration of CR in aqueous solution was determined using a Shimadzu UV-2700 spectrophotometer. Ultraviolet–visible (UV-Vis) absorption spectra were recorded on a PerkinElmer Lambda 1050+ UV/VIS/NIR spectrometer. Optoelectronic properties were evaluated using a CHI660E electrochemical workstation. Steady-state and time-resolved photoluminescence (PL) spectra were collected on an Edinburgh FLS1000 spectrometer. Electron paramagnetic resonance (EPR) spectra were acquired with a Bruker EMXplus-6/1.

4. Adsorption experiments

Typically, 6.0 mg of the sample was added into a 50 mL dried glass vial containing 30.0 mL of CR solution with different initial concentrations. The mixture was stirred at 298 K under dark conditions to avoid photochemical effects. At regular intervals, samples collected from the system were centrifuged at 8000 rpm for 3 minutes. The subsequent supernatant was collected to analyze the CR concentration using a UV-vis spectrophotometer at λ_{max} = 497 nm. The adsorption kinetics were investigated to determine the adsorption capacity and equilibrium time. The effect of solution pH on the adsorption performance was also examined at pH values of 3, 5, 7, 9, and 11.

4.1 Adsorption thermodynamics

6.0 mg of the sample was placed in a 50 mL dried glass vial containing 30.0 mL of

CR solution with initial concentrations of 30, 50, 100, 150, 200, 300, 400, and 500 mg L^{-1}, respectively. The mixtures were magnetically stirred at 600 rpm under dark, and constant-temperature conditions (298 K) for 24 h to reach adsorption equilibrium. Samples collected from the system were centrifuged at 8000 rpm for 3 minutes. The subsequent supernatant was collected to analyze the CR concentration using a UV-vis spectrophotometer at λ_{max} = 497 nm. Then calculated the equilibrium adsorption capacity of the polymer on the adsorbate q_e (mg g^{-1}) according to the equation:

$$q_e = (C_0 - C_e)V/W \qquad \text{(Eq.1)}$$

where q_e is the equilibrium capacity (mg g^{-1}), C_e and C_0 are the equilibrium and initial concentration (mg L^{-1}), V is the solution volume (L), W is the mass of samples (g) respectively. The adsorption isotherms for each sample at a certain temperature were plotted with Ce as the abscissa and q_e as the ordinate.

The adsorption isotherms were fitted by the Langmuir model and the Freundlich model, and the fitting formula is as follows:

Langmuir model:

$$q_e = \frac{q_m K_L C_e}{1 + K_L C_e} \qquad \text{(Eq.2)}$$

where q_e and q_m represent the equilibrium adsorption capacity and the maximum adsorption capacity (mg g^{-1}), C_e represents the equilibrium concentration of the solution, and K_L represents the Langmuir adsorption constant (L mg^{-1}).

Freundlich model:

$$q_e = K_f C_e^{\frac{1}{n}} \qquad \text{(Eq.3)}$$

where K_F ((mg g^{-1})(L mg^{-1})$^{1/n}$) and n represent the Freundlich adsorption constant.

4.2 The kinetic adsorption

6.0 mg of the adsorbent sample was added into 30.0 mL of CR solution with an initial concentration of 300 mg L^{-1}. The system was stirred magnetically at 600 rpm under dark and constant-temperature conditions (298 K). At regular intervals, samples collected from the system were centrifuged at 8000 rpm for 3 minutes. The subsequent supernatant was collected to analyze the CR concentration using a UV-vis spectrophotometer at λ_{max} = 497 nm. When the solution concentration no longer showed significant changes, it was considered that the system had reached adsorption equilibrium, and the equilibrium time was recorded. The adsorption capacity q_e (mg g^{-1}) was then calculated.

4.3 Effect of the solution pH on the adsorption

6.0 mg of the adsorbent sample was added into 30.0 mL of CR solution. The system was stirred magnetically at 600 rpm under constant-temperature (298 K), dark conditions for 120 minutes. The supernatant was then collected, and the absorbance was measured. The effect of the initial pH of the aqueous solution on the adsorption performance was investigated. At 298 K, the concentration of CR in the solution was 300 mg L^{-1}, and the initial pH values were 3, 5, 7, 9, and 11, respectively. The pH of the solution was adjusted using 0.1 M NaOH or HCl aqueous solutions.

4.4 The intra-particle diffusion model

The intra-particle diffusion model by Weber-Morris was further used to fit the kinetic data.

$$q_t = k_{ip}\, t^{1/2} + C \qquad \text{(Eq.4)}$$

where k_{ip} implies the intra-particle diffusion rate (mg g^{-1} $min^{-1/2}$) and C is the constant.

5. Photocatalytic tests

The photocatalytic activity for the degradation of CR under visible light was investigated using a 300 W Xenon lamp equipped with a filter (λ > 420 nm) as the light source. The reaction system was set up in a double circulating beaker with circulating water to maintain the reaction temperature at around 25°C ± 2°C. Before starting the photodegradation, 6.0 mg of the catalyst was added to 30 mL of 300 mg L^{-1} CR solution, and the mixture was stirred in the dark for 60 minutes to ensure adsorption equilibrium. During both the adsorption and degradation processes, samples were taken at regular intervals, and the supernatant was collected. The final concentration of CR was measured using a UV–vis spectrophotometer at λ_{max} = 497 nm. The effect of different pH values on the catalytic degradation was investigated at pH values of 3, 5, 7, 9, and 11. Five cyclic experiments were performed to investigate the stability of COFs on the visible-light photocatalytic degradation of CR. The photodegradation efficiency (R%) and the first order kinetic constant (k) were calculated by the following equations.

$$R\% = (1 - (C_t/C_0)) \times 100\% \qquad \text{(Eq.5)}$$

$$-ln(C_t/C_0) = kt \qquad \text{(Eq.6)}$$

where C_0, C_t and t represent the initial concentration, equilibrium concentration at a certain time and the light irradiation time, respectively.

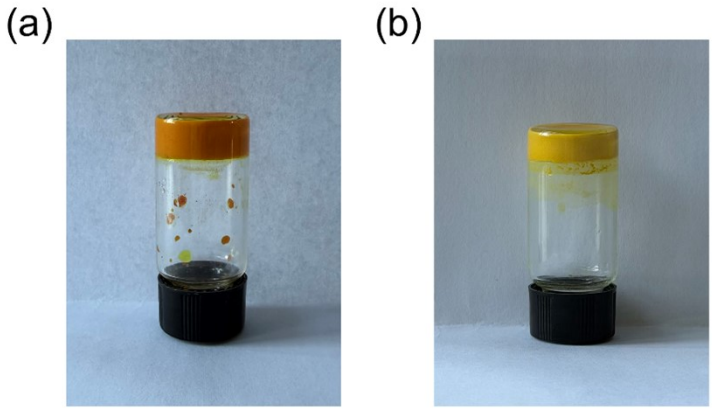

Fig. S1 Photographs showing the rapid gelation of (a) TTP-A and (b) TCA-A.

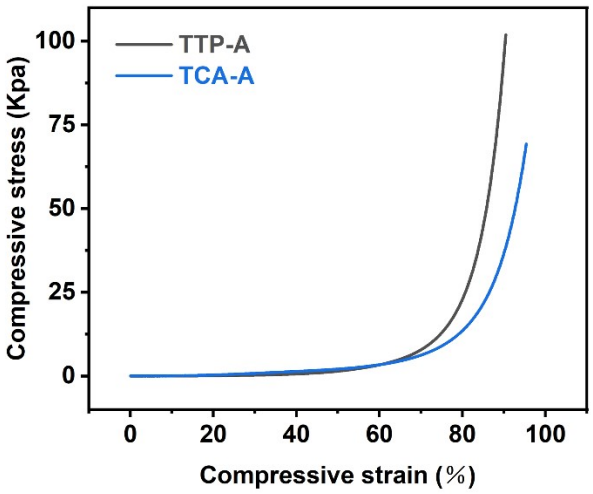

Fig. S2 Compressive stress–strain curves of aerogels.

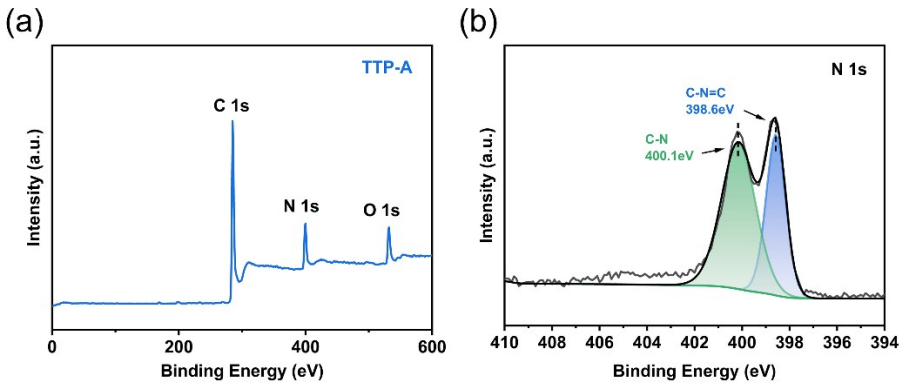

Fig. S3 XPS spectra of TTP-A: (a) Survey, (b) N 1s.

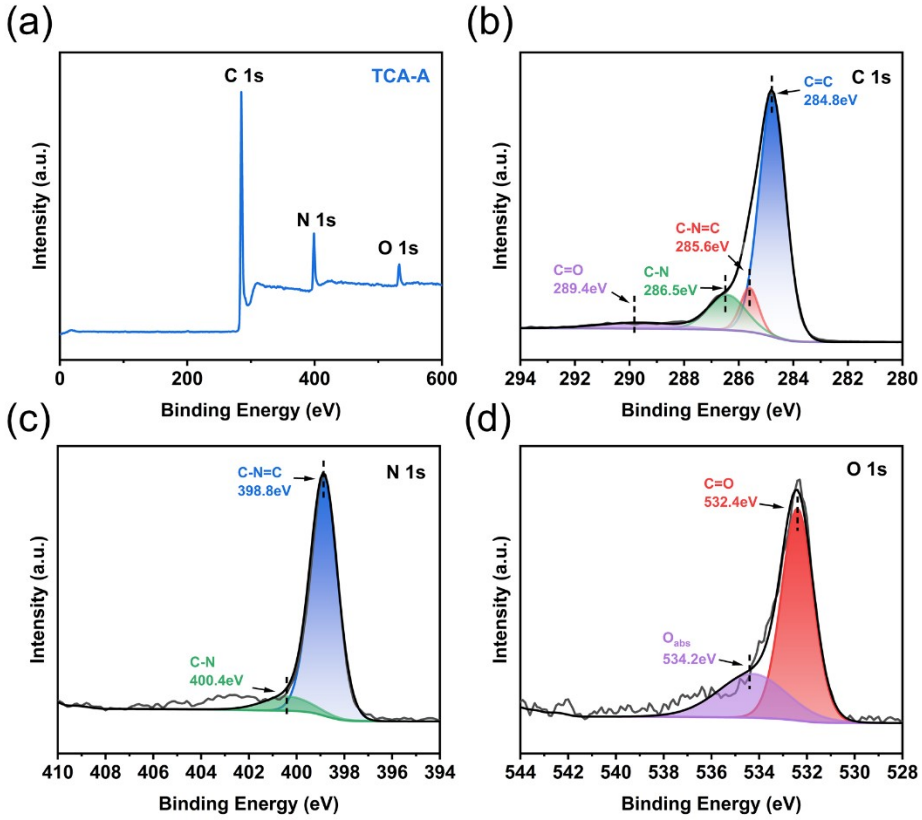

Fig. S4 XPS spectra of TCA-A: (a) Survey, (b) C 1s, (c) N 1s, (d) O 1s.

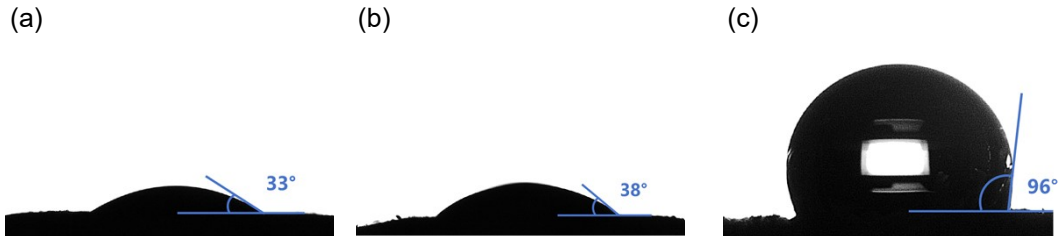

Fig. S5 Water contact angles of (a) TTP-A, (b) TTP-P and (c) TCA-A.

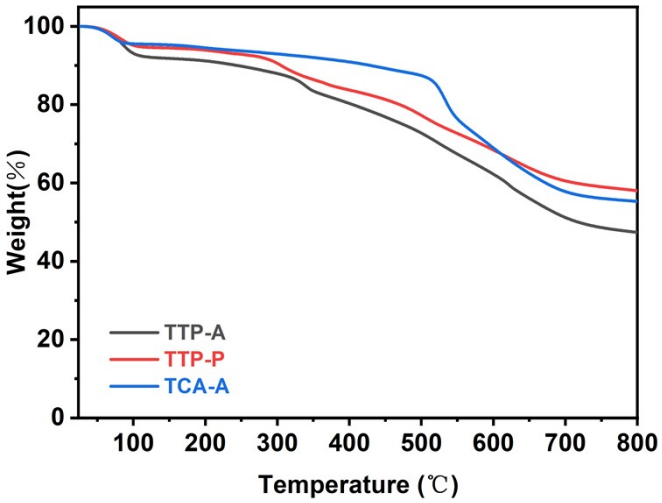

Fig. S6 TGA curves of TTP-A, TTP-P and TCA-A.

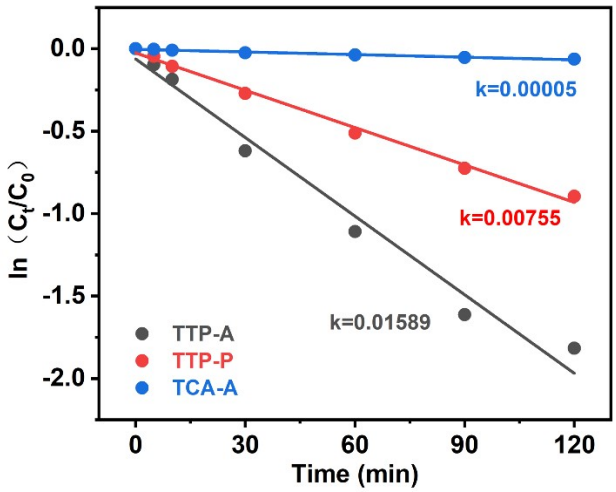

Fig. S7 Corresponding rate constants (k) of CR photodegradation on TTP-A, TTP-P, and TCA-A.

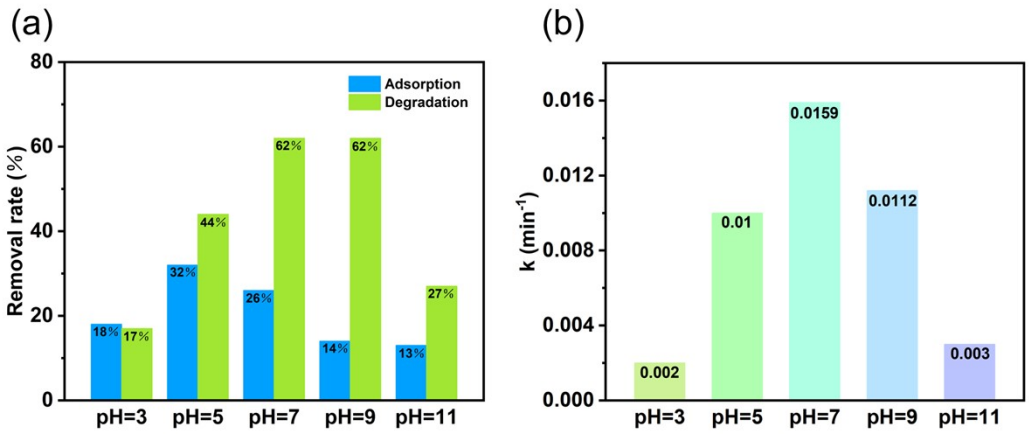

Fig. S8 (a) Adsorption and photocatalytic degradation efficiencies of CR under different pH conditions on TTP-A; (b) Corresponding rate constants (k) of CR photodegradation at different pH values on TTP-A.

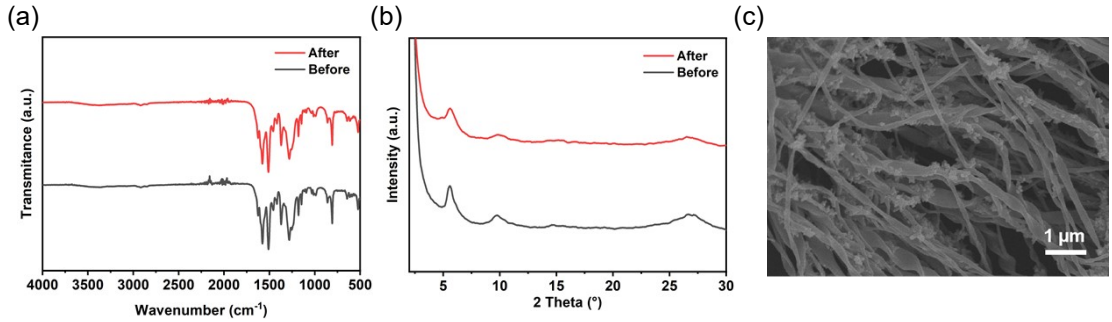

Fig. S9 (a) FT-IR spectra, (b) XRD patterns of TTP-A before and after five cycles; (c) SEM image of TTP-A after five cycles.

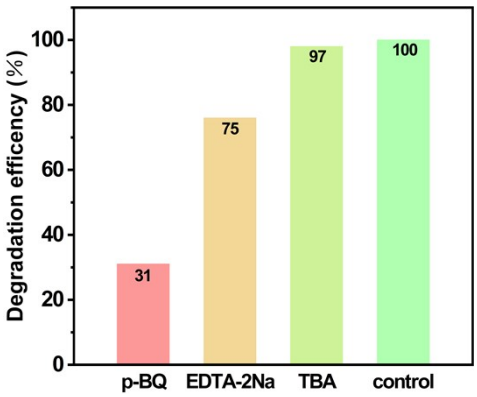

Fig. S10 Contribution of different active species to CR degradation on TTP-A.

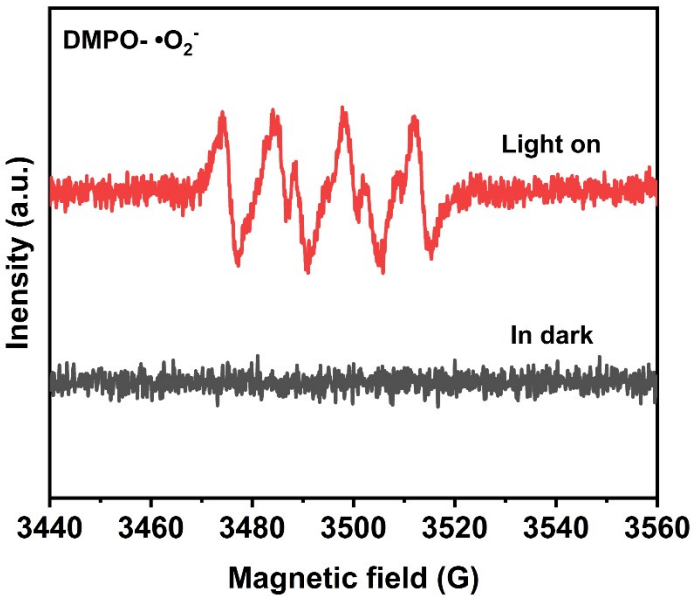

Fig. S11 EPR spectra of DMPO-•O_2^- by TTP-A.

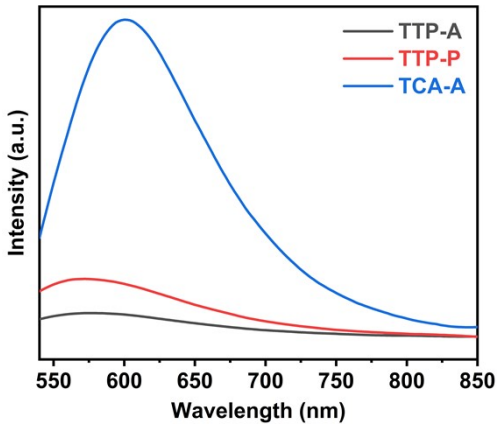

Fig. S12 PL spectra of TTP-A, TTP-P and TCA-A.

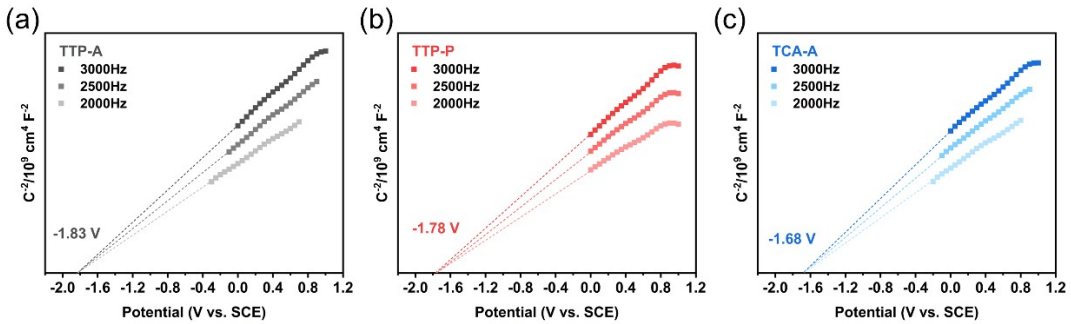

Fig. S13 Mott-Schottky plot of TTP-A, TTP-P and TCA-A.

Tab. S1 Correlated parameters of the equilibrium data for the adsorption of CR on the samples according to the Langmuir and Freundlich model.

Materials	Langmuir model			Freundlich model		
	K_L (L mg^{-1})	q_m (mg g^{-1})	R^2	K_F (mg g^{-1})((L mg^{-1})$^{1/n}$)	n	R^2
TTP-A	0.029	538.95	0.99	138.72	4.57	0.975
TTP-P	0.015	330.66	0.995	51.8	3.5	0.987
TCA-A	0.009	174.76	0.995	12.16	2.45	0.968

Tab. S2 Fitted kinetic parameters for CR adsorption on TTP-A, TTP-P, and TCA-A based on the pseudo-first-order and pseudo-second-order models.

Materials	$q_{e,exp}$ (mg g^{-1})	Pseudo-first-order			Pseudo-second-order		
		$q_{e,cal}$ (mg g^{-1})	k_1 (min^{-1})	R^2	$q_{e,cal}$ (mg g^{-1})	k_2 (g mg^{-1} min^{-1})	R^2
TTP-A	462.5	463.46	0.1453	0.99812	436.68	0.001	0.99971
TTP-P	253.84	229.15	0.093	0.98294	245.1	0.0007	0.99904
TCA-A	124.03	81.01	0.2092	0.96679	120.34	0.0008	0.99703

Tab. S3 Intraparticle diffusion model parameters for CR adsorption on TTP-A and TTP-P.

Materials	K^1_{ip}	K^2_{ip}	K^3_{ip}	C^1	C^2	C^3	R_1^2	R_2^2	R_3^2
TTP-A	75.21	5.58	0.28	34.46	377.01	426.56	0.901	0.957	0.944
TTP-P	36.12	6.77	0.54	9.98	162.23	230.05	0.968	0.96	0.78

Tab. S4 Comparison of adsorption capacity and degradation performance of CR over different materials.

Materials	q_{max} (mg/g)	Initial CR concentration (mg L^{-1})	Catalyst dosage (g L^{-1})	Light source	Degradation time (min)	Degradation efficiency (%)	Ref.
TTP-A	538.95	300	0.2	Xenon lamp (300W, λ > 420 nm)	120	84	This work
CC-ODA POP	103	–	–	–	–	–	1
TPT-TAPT-COF	233	–	–	–	–	–	2
COF-H1	470.3	–	–	–	–	–	3
N-MCA aerogels	431	–	–	–	–	–	4
P-ZrO_2CeO_2ZnO	—	10	1	LED light (20 W, warm white)	250	85.85	5
Bi (5%)/CFs	—	10	0.5	Xenon lamp (300W, λ > 420 nm)	60	97.2	6
Cu_2O/Cu-Ag/AgCl	—	20	0.5	Xenon lamp (500W, λ > 420 nm)	60	92.6	7
$YMnO_3$/wt 10 % $MgAl_2O_4$	122.86	150	1	Xenon lamp (300W, 320–720 nm)	120	98.98	8
TiO_2/CS-2.5 composite aerogels	247.52	200	1	Xenon lamp (300W, UV–Vis)	300	91	9

Not all reported materials provide both adsorption and photocatalytic degradation data for CR. Only the available performance metrics are summarized in this table, while unavailable data are denoted by "–".

References:

1. S. Thottathil, Y. M. Puttaiahgowda, R. Selvaraj, J. G. Elambalassery, R. Vinayagam and T. Varadavenkatesan, *Journal of Molecular Liquids*, 2025, **429**, 127628.
2. P. Panda, A. Warrier and T. Panda, *Microporous and Mesoporous Materials*, 2025, **400,** 113916.
3. G. Hu, G. Cui, J. Zhao, M. Han and R.-Y. Zou, *Polymer Chemistry*, 2022, **13**, 3827-3832.
4. S. Zhai, R. Chen, J. Liu, J. Xu and H. Jiang, *Journal of the Taiwan Institute of Chemical Engineers*, 2021, **120**, 161-168.
5. N. Hokonya, C. Mahamadi, N. Mukaratirwa-Muchanyereyi, T. Gutu and C. Zvinowanda, *Heliyon*, 2022, **8**, e10277.
6. D. Zhang, Z. Xu, H. Zhao, T. Liu, C. An and J. Liu, *Journal of Materials Science*, 2020, **55**, 10765-10772.
7. H. Li, Q. Xia, Y. Zhan, X. Liu, Z. Wang, X. Hu, J. Zhong and W. Gao, *Journal of Alloys and Compounds*, 2024, **1009**, 176952.
8. S. Wang, M. Li, Z. Yin, H. Gao, H. Liu, H. Yang, L. Fang, V. J. Angadi, L. Hu and D. Li, *Advanced Powder Technology*, 2022, **33**, 103771.
9. Y. Du, Z. Wang, Y. Fu, R. Wang, J. An, Y. Gao, X. Gao, H. Wang and C. Shan, *International Journal of Biological Macromolecules*, 2025, **332**, 148641.